J|A|C|S ARTICLES

Published on Web 10/19/2010

High-Resolution ^{19}F MAS NMR Spectroscopy: Structural Disorder and Unusual *J* Couplings in a Fluorinated Hydroxy-Silicate

John M. Griffin,[†] Jonathan R. Yates,[‡] Andrew J. Berry,[§,||] Stephen Wimperis,[⊥] and Sharon E. Ashbrook*[,†]

School of Chemistry and EaStCHEM, University of St. Andrews, North Haugh, St. Andrews KY16 9ST, U.K., Department of Materials, University of Oxford, Parks Road, Oxford OX1 3PH, U.K., Department of Earth Sciences and Engineering, Imperial College London, South Kensington SW7 2AZ, U.K., Department of Mineralogy, Natural History Museum, Cromwell Road, London SW7 5BD, U.K., and School of Chemistry and WestCHEM, University of Glasgow, Glasgow G12 8QQ, U.K.

Received June 29, 2010; E-mail: sema@st-andrews.ac.uk

Abstract: High-resolution ^{19}F magic angle spinning (MAS) NMR spectroscopy is used to study disorder and bonding in a crystalline solid. ^{19}F MAS NMR reveals four distinct F sites in a 50% fluorine-substituted deuterated hydrous magnesium silicate (clinohumite, $4Mg_2SiO_4 \cdot Mg(OD_{1-x}F_x)_2$ with $x = 0.5$), indicating extensive structural disorder. The four ^{19}F peaks can be assigned using density functional theory (DFT) calculations of NMR parameters for a number of structural models with a range of possible local F environments generated by F^-/OH^- substitution. These assignments are supported by two-dimensional ^{19}F double-quantum MAS NMR experiments that correlate F sites based on either spatial proximity (via dipolar couplings) or through-bond connectivity (via scalar, or *J*, couplings). The observation of ^{19}F−^{19}F *J* couplings is unexpected as the fluorines coordinate Mg atoms and the Mg−F interaction is normally considered to be ionic in character (i.e., there is no formal F−Mg−F covalent bonding arrangement). However, DFT calculations predict significant ^{19}F−^{19}F *J* couplings, and these are in good agreement with the splittings observed in a ^{19}F *J*-resolved MAS NMR experiment. The existence of these *J* couplings is discussed in relation to both the nature of bonding in the solid state and the occurrence of so-called "through-space" ^{19}F−^{19}F *J* couplings in solution. Finally, we note that we have found similar structural disorder and spin−spin interactions in both synthetic and naturally occurring clinohumite samples.

Introduction

Structural characterization of crystalline solids has traditionally relied upon diffraction measurements performed on single crystals or powders, as these can provide accurate information about long-range ordering and atomic positions within the unit cell. However, diffraction is less sensitive to atomic-scale effects such as localized disorder (be it positional or compositional), which may be important in determining the bulk physical and chemical properties of a material. In this respect, the high sensitivity of solid-state nuclear magnetic resonance (NMR) spectroscopy (and in particular of the NMR chemical shift) to the local chemical environment makes it a powerful complementary tool to diffraction-based methods for the investigation of disordered systems. In many cases, distinct spectral resonances are observed which, once assigned, can provide both qualitative and quantitative information on the nature of the disorder present.

The ^{19}F nucleus, with spin quantum number $I = 1/2$ and a high receptivity (100% natural abundance and a gyromagnetic ratio similar to that of ^{1}H), would appear to be well-suited for NMR investigations in solids. Furthermore, the large ^{19}F chemical shift range (~800 ppm, compared with the ~20 ppm typically found for ^{1}H) results in spectra which are particularly sensitive to relatively small changes in local environment. Indeed, solid-state ^{19}F NMR has been used for structural studies of a range of complex and disordered materials.[1] The high natural abundance of ^{19}F also makes it a convenient choice for the application of multidimensional correlation experiments,[2] where magnetization is transferred between pairs of spins (either heteronuclear or homonuclear) in an attempt to assign spectra

[†] University of St. Andrews.
[‡] University of Oxford.
[§] Imperial College London.
[||] Natural History Museum.
[⊥] University of Glasgow.

(1) (a) Stebbins, J. F.; Zeng, Q. *J. Non-Cryst. Sol.* **2000**, *262*, 1. (b) Zeng, Q.; Stebbins, J. F. *Am. Mineral.* **2000**, *85*, 863. (c) Chan, C. C.; Eckert, H. *J. Non-Cryst. Sol.* **2001**, *284*, 16. (d) Body, M.; Silly, G.; Legein, C.; Buzaré, J.-Y. *Inorg. Chem.* **2004**, *43*, 2474. (e) Martineau, C.; Body, M.; Legein, C.; Silly, G.; Buzaré, J.-Y.; Fayon, F. *Inorg. Chem.* **2006**, *45*, 10215.

(2) (a) Martineau, C.; Fayon, F.; Legein, C.; Buzaré, J.-Y.; Body, M.; Massiot, D.; Goutenoire, F. *Dalton Trans.* **2008**, 6150. (b) Martineau, C.; Fayon, F.; Legein, C.; Buzaré, J.-Y.; Goutenoire, F.; Suard, E. *Inorg. Chem.* **2008**, *47*, 10895. (c) Martineau, C.; Legein, C.; Buzaré, J.-Y.; Fayon, F. *Phys. Chem. Chem. Phys.* **2009**, *11*, 950. (d) Wang, Q.; Hu, B.; Fayon, F.; Trebosc, J.; Legein, C.; Lafon, O.; Deng, F.; Amoureux, J.-P. *Phys. Chem. Chem. Phys.* **2009**, *11*, 10391. (e) Wang, Q.; Hu, B.; Lafon, O.; Trebosc, J.; Deng, F.; Amoureux, J.-P. *J. Magn. Reson.* **2010**, *203*, 113.

and determine the local atomic environment. Such experiments can usually be adapted to investigate either through-space or through-bond connectivities, depending upon whether internuclear transfer is through the dipolar (*d*) or scalar (*J*) coupling. However, the high natural abundance and large gyromagnetic ratio of ^{19}F can result in very strong homonuclear dipolar couplings that may hinder the resolution of distinct sites and the extraction of site-specific information. This can be overcome by fast magic angle spinning (MAS), with the recent introduction of commercial probeheads able to achieve MAS rates between 60 and 70 kHz offering routine acquisition of high-resolution spectra for materials with strong dipolar couplings.[3] Furthermore, this also offers, perhaps for the first time, the opportunity to exploit the scalar couplings in such materials. This interaction, although usually smaller than the dipolar coupling, offers both a more selective transfer and potential information about the nature of bonding interactions in the solid state.

A further recent advance in methodology has been the development of density functional theory (DFT) codes that utilize periodic boundary conditions. These codes enable efficient calculation of solid-state NMR parameters with high accuracy, exploiting the inherent periodicity associated with crystalline materials. In particular, codes using the gauge including projector augmented wave (or GIPAW)[4] approach, such as CASTEP,[5] have seen widespread applications to a large range of systems,[6] being applied, for example, to the calculation of ^{19}F NMR parameters for a range of inorganic fluorides.[7] More recently, this approach has been extended to enable the calculation of spin−spin scalar couplings.[8] The calculation of *J* couplings from first principles offers not only a predictive tool to aid the implementation of experiments which utilize these couplings, but also new possibilities for the interpretation of NMR spectra obtained by such methods.[9]

In this work we combine high-resolution ^{19}F MAS NMR with the calculation of ^{19}F NMR parameters from first principles for the study of disorder in the magnesium silicate clinohumite ($4Mg_2SiO_4 \cdot Mg(F,OH)_2$). This mineral shares close structural similarities with forsterite (Mg_2SiO_4)[10,11] and is of considerable interest as a possible model for the incorporation of water within the Earth's upper mantle.[11,12] In contrast to hydroxyl-clinohumite ($4Mg_2SiO_4 \cdot Mg(OH)_2$), where recent work has highlighted the presence of a dynamic disorder of the OH hydrogen atoms between two distinct sites,[12−15] diffraction studies of fluorine-rich clinohumite show a single hydrogen site arising from the formation of O−H···F hydrogen bonds,[16,17] which inhibits the dynamic exchange of the hydroxyl protons. Although this indicates some degree of local ordering in the fluorine substitution, the positions of F^- and OH^- are not distinguished in the refinement of the diffraction data. In the current study, ^{19}F NMR spectral interpretation and assignment of clinohumite is aided by the use of first-principles DFT calculations and two-dimensional homonuclear correlation experiments. The use of fast MAS rates enables the identification of scalar couplings between fluorine species that would not typically be described as "bonded" in the conventional chemical sense, and we suggest that the mechanism of these *J* couplings has a significant "through-space" component, unlike more commonly observed *J* couplings that are generally considered to be mediated via the electrons in covalent bonds.

Experimental and Computational Details

Synthesis. A sample of deuterated clinohumite with a target composition of $4Mg_2SiO_4 \cdot Mg(OD_{1-x}F_x)_2$ with $x = 0.5$ (hereafter referred to as $F_{0.5}(OD)_{0.5}$-clinohumite) was prepared from a stoichiometric mix of SiO_2, MgO, and MgF_2, plus excess D_2O (5 wt %) in a sealed Pt capsule at 20 kbar and 1000 °C using a NaCl/pyrex/MgO pressure assembly and a piston-cylinder apparatus. No impurity phases were detected by X-ray diffraction. The composition of the product (20−30 μm crystal was determined using a Cameca SX-100 electron microprobe (15 kV, 20 nA, 5 μm analysis spot) to be $Mg_{9.02}Si_{3.98}O_{16}F_{1.08}(OD)_{0.92}$ (24 analyses). A faceted gem-quality crystal of natural clinohumite from Pamir, Tajikistan, was obtained commercially. The composition of this sample was determined from 45 electron microprobe analyses to be $Mg_{8.85}Fe_{0.01}Ti_{0.2}(Si_{3.94}O_{16})O_{0.4}F_{0.97}(OH)_{0.63}$ (operating conditions as above). Forsterite (Mg, Si), rutile (Ti), fayalite (Fe), and topaz (F) were used as standards, and OD/OH ratios were calculated from stoichiometry on the basis of 13 cations.

Solid-State NMR. Solid-state NMR experiments were performed on a Bruker Avance III spectrometer operating at a magnetic field

(3) (a) Bertini, I.; Emsley, L.; Lelli, M.; Luchinat, C.; Mao, J. F.; Pintacuda, G. *J. Am. Chem. Soc.* **2010**, *132*, 5558. (b) Xue, X.; Kanzaki, M. *J. Am. Ceram. Soc.* **2009**, *92*, 2803. (c) Amoureux, J. P.; Hu, B.; Trebosc, J. *J. Magn. Reson.* **2008**, *193*, 305.

(4) Pickard, C. J.; Mauri, F. *Phys. Rev. B* **2001**, *63*, 245101.

(5) (a) Segall, M. D.; Lindan, P. J. D.; Probert, M. J.; Pickard, C. J.; Hasnip, P. J.; Clark, S. J.; Payne, M. C. *J. Phys. Condens. Matter* **2002**, *14*, 2717. (b) Clark, S. J.; Segall, M. D.; Pickard, C. J.; Hasnip, P. J.; Probert, M. J.; Refson, K.; Payne, M. C. *Z. Kristallogr.* **2005**, *220*, 567.

(6) (a) Harris, R. K.; Joyce, S. A.; Pickard, C. J.; Cadars, S.; Emsley, L. *Phys. Chem. Chem. Phys.* **2006**, *8*, 137. (b) Ashbrook, S. E.; Le Polles, L.; Pickard, C. J.; Berry, A. J.; Wimperis, S.; Farnan, I. *Phys. Chem. Chem. Phys.* **2007**, *9*, 1587. (c) Ashbrook, S. E.; Berry, A. J.; Frost, D. J.; Gregorovic, A.; Pickard, C. J.; Readman, J. E.; Wimperis, S. *J. Am. Chem. Soc.* **2007**, *129*, 13213. (d) Pourpoint, F.; Gervais, C.; Bonhomme-Coury, L.; Azais, T.; Coelho, C.; Mauri, F.; Alonso, B.; Babonneau, F.; Bonhomme, C. *Appl. Magn. Reson.* **2007**, *32*, 435. (e) Ashbrook, S. E.; Cutajar, M.; Pickard, C. J.; Walton, R. I.; Wimperis, S. *Phys. Chem. Chem. Phys.* **2008**, *10*, 5754. (f) O'Dell, L.; Schurko, R. W. *Phys. Chem. Chem. Phys.* **2009**, *11*, 7069. (g) Chapman, R. P.; Bryce, D. *Phys. Chem. Chem. Phys.* **2009**, *11*, 6987. (h) Pallister, P. J.; Moudrakovski, I. L.; Ripmeester, J. A. *Phys. Chem. Chem. Phys.* **2009**, *11*, 11487. (i) Reader, S. W.; Mitchell, M. R.; Johnston, K. E.; Pickard, C. J.; Whittle, K. R.; Ashbrook, S. E. *J. Phys. Chem. C* **2009**, *113*, 18874.

(7) Zheng, A.; Liu, S.-B.; Deng, F. *J. Phys. Chem. C* **2009**, *113*, 15018.

(8) (a) Joyce, S. A.; Yates, J. R.; Pickard, C. J.; Mauri, F. *J. Chem. Phys.* **2007**, *127*, 204107. (b) Joyce, S. A.; Yates, J. R.; Pickard, C. J.; Brown, S. P. *J. Am. Chem. Soc.* **2008**, *130*, 12663.

(9) (a) Hung, I.; Uldry, A.-C.; Becker-Baldus, J.; Webber, A. L.; Wong, A.; Smith, M. E.; Joyce, S. A.; Yates, J. R.; Pickard, C. J.; Dupree, R.; Brown, S. P. *J. Am. Chem. Soc.* **2009**, *131*, 1820. (b) Cadars, S.; Brouwer, D. H.; Chmelka, B. F. *Phys. Chem. Chem. Phys.* **2009**, *11*, 1825. (c) Bonhomme, C.; Gervais, C.; Coelho, C.; Pourpoint, F.; Azais, T.; Bonhomme-Coury, L.; Babonneau, F.; Jacob, G.; Ferrari, D.; Canet, D.; Yates, J. R.; Pickard, C. J.; Joyce, S. A.; Mauri, F.; Massiot, D. *Magn. Reson. Chem.* **2010**, in press. (d) Yates, J. R. *Magn. Reson. Chem.* **2010**, in press. (e) Bryce, D. *Magn. Reson. Chem.* **2010**, in press.

(10) Kitamura, M.; Kondoh, S.; Morimoto, N.; Miller, G. H.; Rossman, G. R.; Putnis, A. *Nature* **1987**, *328*, 143.

(11) Ashbrook, S. E.; Berry, A. J.; Wimperis, S. *Am. Mineral.* **1999**, *84*, 1191.

(12) Ashbrook, S. E.; Berry, A. J.; Wimperis, S. *J. Am. Chem. Soc.* **2001**, *123*, 6360.

(13) Ashbrook, S. E.; Antonijevic, S.; Berry, A. J.; Wimperis, S. *Chem. Phys. Lett.* **2002**, *364*, 634.

(14) Griffin, J. M.; Wimperis, S.; Berry, A. J.; Pickard, C. J.; Ashbrook, S. E. *J. Phys. Chem. C.* **2009**, *113*, 465.

(15) Griffin, J. M.; Miller, A. J.; Wimperis, S.; Berry, A. J.; Ashbrook, S. E. *Phys. Chem. Chem. Phys.* **2010**, *12*, 2989.

(16) Friederich, A.; Lager, G. A.; Kunz, M.; Chakoumakos, B. C.; Smyth, J. R.; Schultz, A. J. *Am. Mineral.* **2001**, *86*, 981.

(17) Friederich, A.; Lager, G. A.; Ulmer, P.; Kunz, M.; Marshall, W. G. *Am. Mineral.* **2002**, *87*, 931.

strength, B_0, of 14.1 T, corresponding to a ^{19}F Larmor frequency, ν_0, of 564.7 MHz. Experiments were performed using either Bruker 2.5-mm or 1.3-mm double resonance H/F X probes, with MAS rates (ν_R) of 30 kHz or 60 kHz, respectively. Chemical shifts are given relative to CCl_3F, referenced using a secondary reference of polytetrafluoroethylene (PTFE) ($\delta = -122.7$ ppm). Typical recycle intervals were 8 s. Two-dimensional homonuclear ^{19}F correlation experiments were carried out using either (i) the double-quantum (DQ) MAS pulse sequence in ref 18 with one cycle of BABA[19] dipolar recoupling for DQ excitation and reconversion or (ii) the refocused-INADEQUATE pulse sequence given in ref 20 with a rotor-synchronized J evolution period, τ, of 20 ms. ^{19}F J-resolved experiments were performed using the pulse sequence described in ref 21, which employs a z-filter prior to acquisition to ensure pure absorption-mode line shapes. Rotor-synchronized $t_1/2$ increments of 4 ms were used. In the two-dimensional experiments, presaturation trains of 32 pulses were used to reduce the overall acquisition time of the experiment. Note that the use of deuteration also suppresses ^{1}H/^{1}H dipolar couplings and increases T_2' (by up to a factor of 6 for the F_A resonance) as compared to a protonated sample of similar composition, easing the observation of scalar couplings. Full experimental details, desired coherence transfer pathways, and the phase cycles employed are given in the Supporting Information. In all experiments, the spinning angle was accurately adjusted to the magic angle using the OD resonance in the ^{2}H MAS NMR spectrum of fully deuterated malonic acid.

Calculations. Calculations of NMR parameters and J couplings were carried out using the CASTEP DFT code,[5] employing the GIPAW algorithm[4] which allows the reconstruction of the all-electron wave function in the presence of a magnetic field. The generalized gradient approximation (GGA) PBE functional[22] was employed, and core−valence interactions were described by ultrasoft pseudopotentials.[23,24] A planewave energy cutoff of 50 Ry (680 eV) was used, and integrals over the Brillouin zone were performed using a k-point spacing of 0.05 Å^{-1}. Calculations generate the absolute shielding tensor ($\boldsymbol{\sigma}$) in the crystal frame. Diagonalization of the symmetric part of $\boldsymbol{\sigma}$ yields the three principal components, σ_{XX}, σ_{YY}, and σ_{ZZ}. The isotropic shielding, σ_{iso}, is given by $(1/3)\mathrm{Tr}\{\boldsymbol{\sigma}\}$, while the magnitude ($\Delta_{CS}$) and asymmetry ($\eta_{CS}$) of the chemical shift anisotropy (CSA) can be calculated from the principal components by $\Delta_{CS} = \sigma_{ZZ} - \sigma_{iso}$ and $\eta_{CS} = (\sigma_{YY} - \sigma_{XX})/(\sigma_{ZZ} - \sigma_{iso})$, where $|\sigma_{ZZ} - \sigma_{iso}| \geq |\sigma_{XX} - \sigma_{iso}| \geq |\sigma_{YY} - \sigma_{iso}|$. The isotropic chemical shift, δ_{iso}, is given (assuming $\sigma_{ref} \ll 1$) by $-(\sigma_{iso} - \sigma_{ref})$, where σ_{ref} is a reference shielding (81.4 ppm). This value was determined by comparison between calculated ^{19}F isotropic shieldings and experimental literature values for ^{19}F isotropic chemical shifts for 20 simple fluorine-containing compounds. These results indicated that it was necessary to apply a scaling factor ($k = 0.68$) to the calculated values to match experiment and enable the accurate prediction of ^{19}F chemical shifts. For full details of these calculations, see Supporting Information.

For calculations on clinohumite, the initial atomic positions and unit cell parameters were taken from a neutron powder diffraction structure.[25] Prior to calculation of the NMR parameters, however, full geometry optimizations were performed (also using a cutoff energy of 50 Ry and k-point spacing of 0.05 Å^{-1}), where both the lattice parameters and internal atomic coordinates were allowed to vary. For the calculation of some fluorine environments, the construction of $2 \times 1 \times 1$ and $3 \times 1 \times 1$ supercells was necessary. Calculations were performed using the EaStCHEM Research Computing Facility, which consists of 136 AMD Opteron 280 dual-core processors running at 2.4 GHz, partly connected by Infinipath high speed interconnects. Calculation wallclock times ranged from 9 to 75 h using four cores, depending on the size of the model unit cell used in the calculation.

Scalar couplings were calculated for fully fluorinated clinohumite ($4Mg_2SiO_4 \cdot MgF_2$) with a developer's version of the CASTEP[5] code, using the approach introduced in ref 8. This enables the calculation of J couplings tensors for crystalline systems using the planewave pseudopotential formalism of DFT. The basis set contained planewaves up to a maximum kinetic energy of 90 Ry, and integrals over the Brillouin zone were performed using a k-point spacing of 0.1 Å^{-1}. The PBE density functional was employed, and the core−valence interactions described with Troullier−Martins norm-conserving pseudopotentials.[26] The J coupling is obtained by considering the perturbation between the magnetic moment of a chosen atom and the other atoms in the cell. This perturbation breaks the translational symmetry, and therefore a $3 \times 1 \times 1$ supercell was used to eliminate the interaction between periodic images of the perturbing atom. Diagonalization of the symmetric part of the tensor, $\mathbf{J}$, yields the principal components such that $|J_{ZZ} - J_{iso}| \geq |J_{XX} - J_{iso}| \geq |J_{YY} - J_{iso}|$, where the isotropic J coupling, J_{iso}, is given by $(1/3)\mathrm{Tr}\{\mathbf{J}\}$. The anisotropy, ΔJ, is defined as $\Delta J = J_{ZZ} - (J_{XX} + J_{YY})/2$. Calculations were performed at the Oxford Supercomputer Centre and took a wallclock time of 13 h on 16 dual-core Intel Xeon 5130 processors running at 2.0 GHz.

Results and Discussion

The structure of clinohumite can be described as four forsterite-like layers (Mg_2SiO_4) alternating with a fluorine-substituted hydrated layer ($Mg(F,OH)_2$) that lies in the plane parallel to the a and b axes, as shown schematically in Figure 1a. Diffraction studies have identified a centrosymmetric pair of hydrogen positions that correspond to a single hydrogen site.[16,17] These positions, denoted H1, are separated by a distance of ~1 Å, meaning that the simultaneous occupancy of two adjacent H1 sites is a highly unstable configuration. For hydroxyl-clinohumite ($4Mg_2SiO_4 \cdot Mg(OH)_2$), the end member of the solid solution, a second crystallographically distinct hydrogen site (H2) has been identified.[25] The occupancy of the two distinct sites has been shown (by diffraction) to be ~50%, suggesting a disordered material, where the unfavorable interactions between the proximate H1 species are therefore eliminated. However, recent work using NMR spectroscopy has revealed the presence of a dynamic, not a static, disorder of the hydrogen positions at room temperature, with the effects of microsecond-time scale exchange observed in both ^{17}O and ^{2}H spectra.[11−15] Although hydroxyl-clinohumite has been found in nature,[27] in most natural samples, substitution of fluoride anions for hydroxyl groups usually reduces the amount of hydrogen and, therefore, the occupancy of the single hydrogen site to ~50% or less. This avoids the close proximity of the hydroxyl groups, and enables the formation of OH···F$^-$ hydrogen bonds, as shown in Figure 1b. A recent ^{2}H NMR investigation of fluorinated deuterated clinohumite ($F_{0.5}(OD)_{0.5}$-clinohumite as described above) demonstrated that the dynamics previously observed for the hydroxyl end member were not present in this substituted mineral,[15] suggesting an ordered incorporation of fluorine, with all deuterons situated on the H1 site.

(18) Geen, H.; Titman, J. J.; Gottwald, J.; Spiess, H. W. *Chem. Phys. Lett.* **1994**, *227*, 79.
(19) Sommer, W.; Gottwald, J.; Demco, D. E.; Spiess, H. W. *J. Magn. Reson., Ser. A* **1995**, *113*, 131.
(20) Fayon, F.; Levitt, M. H.; Titman, J. J.; Gregory, D. H.; Duma, L.; Emsley, L.; Brown, S. P. *J. Chem. Phys.* **2005**, *122*, 194313.
(21) Brown, S. P.; Pérez-Torralba, M.; Sanz, D.; Claramunt, R. M.; Emsley, L. *Chem. Commun.* **2002**, 1852.
(22) Perdew, J. P.; Burke, K.; Ernzerhof, M. *Phys. Rev. Lett.* **1996**, *77*, 3865.
(23) Vanderbilt, D. *Phys. Rev. B* **1990**, *41*, 7892.
(24) Yates, J. R.; Pickard, C. J.; Mauri, F. *Phys. Rev. B* **2007**, *76*, 024401.
(25) Berry, A. J.; James, M. *Am. Mineral.* **2001**, *86*, 181.
(26) Troullier, N.; Martins, J. L. *Phys. Rev. B* **1991**, *43*, 1991.
(27) Ferraris, G.; Prencipe, M.; Sokolova, E. V.; Gekimyants, V. M.; Spiridonov, E. M. *Z. Kristallogr.* **2000**, *215*, 169.

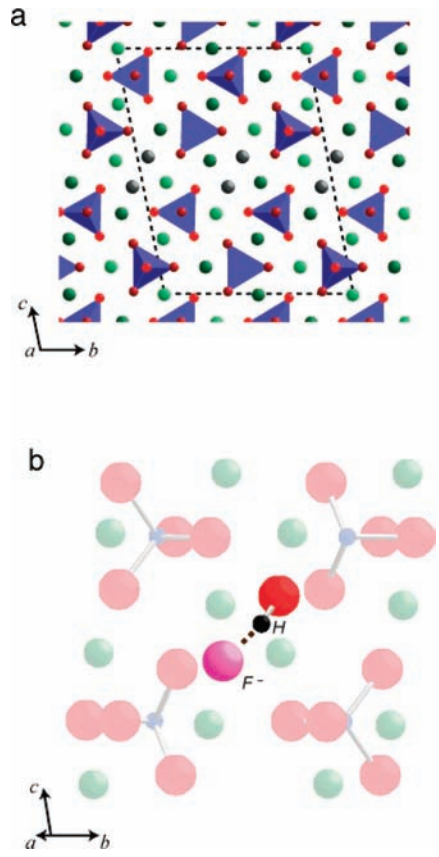

Figure 1. (a) Schematic view of the structure of clinohumite $4Mg_2SiO_4 \cdot Mg(OH,F)_2$, with SiO_4^{4-} groups represented by blue tetrahedra, magnesium atoms in green, and oxygen atoms in red. Fluorine/hydroxyl oxygen sites are shown in gray. Shading indicates height within the structure. Hydroxyl protons/deuterons are omitted for clarity. The unit cell is indicated by dashed lines. (b) The $OH\cdots F^-$ hydrogen bond that results from the substitution of fluoride ions into the clinohumite structure.

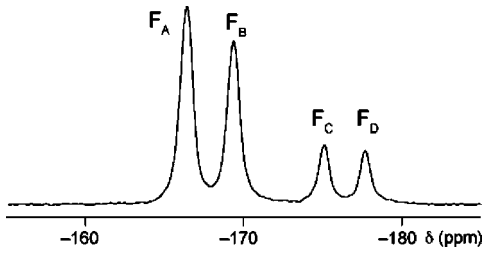

Figure 2. ^{19}F MAS NMR spectrum of $F_{0.5}(OD)_{0.5}$-clinohumite recorded with $\nu_R = 30$ kHz. The peak assignments refer to the local environments shown in Figure 3b.

The ^{19}F MAS NMR spectrum of $F_{0.5}(OD)_{0.5}$-clinohumite, recorded with $\nu_R = 30$ kHz, shown in Figure 2 exhibits four well-resolved resonances of similar line width, with isotropic chemical shifts, δ, of −166.4, −169.3, −175.1, and −177.7 ppm and relative intensities of 42.6%, 35.7%, 11.5%, and 10.2%, respectively. This suggests (in contrast to the ordered incorporation described above) a degree of structural disorder, with distinct local fluorine environments present. If the clinohumite structure is considered in more detail, it can be seen that within the hydrated layer the OD^-/F^- sites (shown in gray) form a staggered chain lying parallel to the *a* axis, as shown in Figure 3a. For any F^- anion, a number of different local environments are possible, depending upon the nature of the anions at nearby OD^-/F^- sites. The two closest sites lie at distances of ∼2.7 and ∼3.2 Å, respectively, with two additional (equidistant) sites

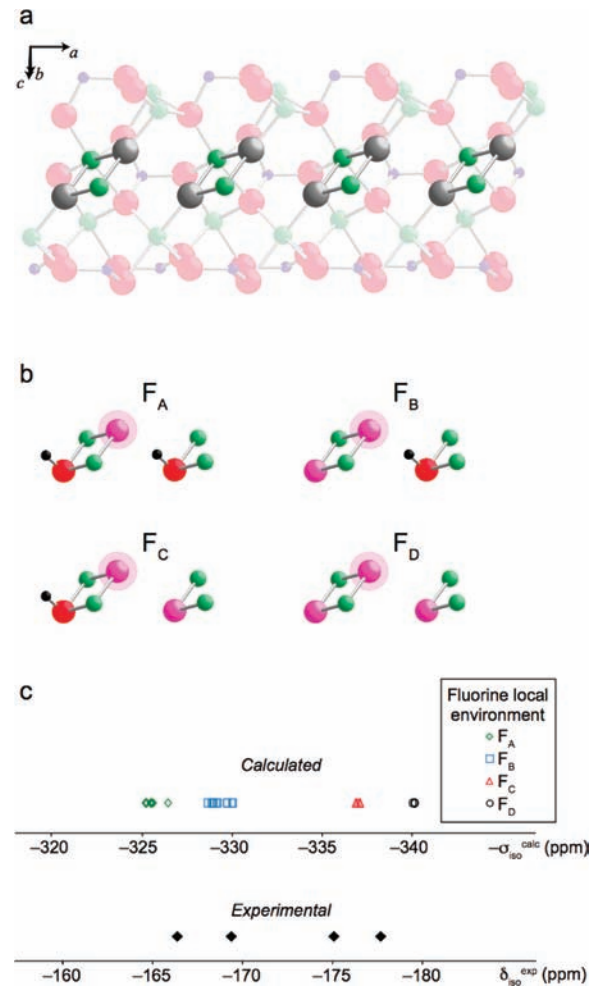

Figure 3. (a) View of the clinohumite crystal structure showing the staggered arrangement of F^-/OH^- sites. Silicon, magnesium, and oxygen atoms are shown in blue, green, and red, respectively. Fluorine/hydroxyl oxygen sites are shown in gray. (b) Four possible local fluorine environments in clinohumite with varying substitutions of OH^-/F^-, denoted F_A−F_D. Fluorine, oxygen, magnesium, and hydrogen/deuterium are shown in pink, red, green, and black, respectively. (c) Comparison of calculated ^{19}F isotropic shieldings, $-\sigma_{iso}^{calc}$, and experimental ^{19}F chemical shifts, δ_{iso}^{exp}. Calculated shieldings are for a range of clinohumite structures substituted at varying amounts and positions with fluorine, as described in more detail in the Supporting Information.

at ∼4.8 Å, and five further sites over 5.1 Å away. If only the two closest sites are considered, and assuming these can be occupied either by OD^- or by F^-, four different local fluorine environments would be possible, denoted F_A to F_D, as shown in Figure 3b. (Note that in each case the longer-range environment may be different if the substitution of the more remote OD^-/F^- sites is also considered). Of these four environments, only F_A and F_B maximize the number of $OD\cdots F^-$ hydrogen-bonded pairs. The F_C and F_D environments contain adjacent fluoride anions, thus inhibiting the formation of a hydrogen bond. These types of environment would perhaps be expected to occur when the level of fluorine substitution was greater than 50%; indeed the F_D environment is that which would be found in fully fluorinated clinohumite.

To gain insight into the ^{19}F chemical shifts expected for the environments shown in Figure 3b, a range of first-principles calculations were performed, with F^- and OH^- anions substituted into a unit cell (or $2 \times 1 \times 1$ and $3 \times 1 \times 1$ supercells) of clinohumite, generating all possible local fluorine environ-

Table 1. Experimental ^{19}F Chemical Shift, δ_{iso}^{exp}, and Average Calculated ^{19}F NMR Parameters (isotropic shielding $\langle\sigma_{iso}^{calc}\rangle$, Isotropic Chemical Shift, $\langle\delta_{iso}^{calc,scaled}\rangle$, Chemical Shift Anisotropy, $\langle|\Delta_{CS}^{calc,scaled}|\rangle$, and Asymmetry, $\langle\eta_{CS}^{calc}\rangle$) for the Four Fluorine Environments Shown in Figure 3b

species	δ_{iso}^{exp} (ppm)	$\langle\sigma_{iso}^{calc}\rangle$ (ppm)	$\langle\delta_{iso}^{calc,scaled}\rangle^a$ (ppm)	$\langle\|\Delta_{CS}^{calc,scaled}\|\rangle^b$ (ppm)	$\langle\eta_{CS}^{calc}\rangle$
F_A	−166.4	325.5	−166.6	6.3	0.64
F_B	−169.3	329.3	−169.2	5.2	0.68
F_C	−175.1	337.0	−174.4	8.3	0.98
F_D	−177.7	340.1	−176.6	7.8	0.62

[a] Chemical shifts are calculated by $\delta_{iso}^{calc,scaled} = -k(\sigma_{iso}^{calc} - \sigma_{ref})$ where σ_{ref} is 81.4 ppm, and the scaling factor, k, is 0.68. See Supporting Information. [b] Calculated values of the CSA are also scaled by k = 0.68. See Supporting Information.

ments. For full details of these calculations and the exact structural models used, see Supporting Information. The results are summarized in Figure 3c, where the calculated isotropic shieldings (plotted as $-\sigma_{iso}^{calc}$) are shown alongside the experimental chemical shifts. Four distinct shift ranges are observed, with the nature of the two closest anionic species being the principal factor that determines the shielding. The relative differences in calculated shielding agree well with those observed experimentally and enable a tentative assignment of the ^{19}F MAS NMR spectrum, as shown in Figure 2. Differences in the longer-range environment result in much smaller changes in shielding within each of the four main groups, consistent with the broadening of the experimental spectral resonances. For each of the four fluorine environments, the average (mean) calculated values of $\sigma_{iso,}$, δ_{iso}, Δ_{CS}, and η_{CS} are given in Table 1.

The F_A and F_B environments shown in Figure 3b are consistent with the formation of OD···F$^-$ hydrogen-bonded pairs (and therefore a degree of short-range order in the structure). These account for the majority of the spectral intensity (∼78%) in the ^{19}F MAS spectrum in Figure 2. However, the presence of both environments within the spectrum suggest that there is little or no longer-range order in the structure, i.e., which of the two OD$^-$/F$^-$ sites within a pair is occupied by F$^-$ and which by OD$^-$ is not well correlated between different pairs. In contrast, the F_C and F_D environments prevent the formation of hydrogen-bonded pairs and so may be expected to be present if (i) the substitution level of F is greater than 50% or (ii) there are regions of the material that are locally more fluorine rich. As the electron microprobe analysis revealed the substitution level to be only slightly above 50% (∼54%), only a small number of F_C and F_D environments are expected to be present. However, these account for ∼22% of the total spectral intensity in Figure 2, suggesting that, although there is a preference for the formation of OD···F$^-$ hydrogen-bonded pairs (no preference would result in equal proportions of all types of F environment), the material is not fully ordered in this way, and that both fluorine rich and fluorine deficient regions are present. In the latter case, the destabilizing interaction between adjacent hydroxyl deuterons could be avoided by a two-site dynamic exchange process as in hydroxyl-clinohumite.[14,15] However, in a previous ^{2}H MAS NMR study of this material[15] the motional line broadening that is indicative of this exchange was not observed, though it may be difficult to observe a low intensity, broadened line shape in the presence of the more intense and sharper resonance.

To support the conclusions drawn from the computational studies regarding the spectral assignment, a number of two-dimensional correlation experiments, where magnetization is

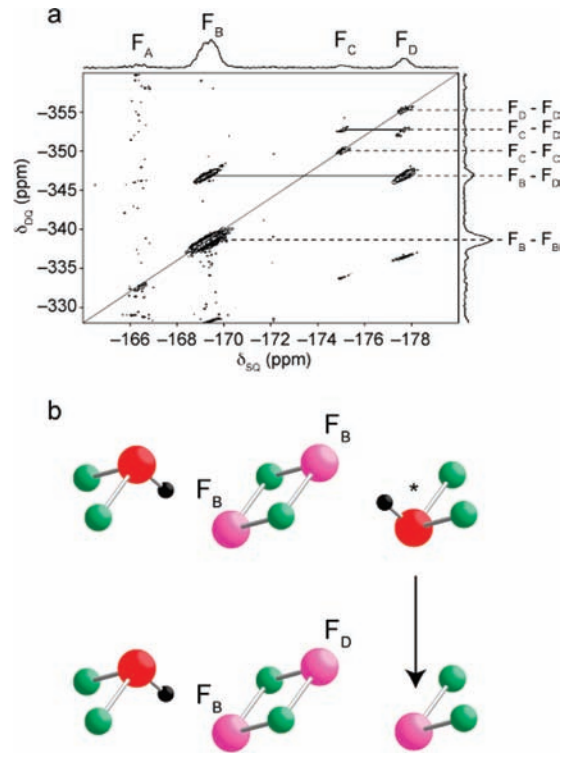

Figure 4. (a) Rotor-synchronized ^{19}F through-space DQ MAS NMR spectrum of $F_{0.5}(OD)_{0.5}$-clinohumite, and corresponding projections, recorded using one cycle of BABA recoupling, with ν_R = 30 kHz. The diagonal line shows the axis $\delta_{DQ} = 2\delta_{SQ}$, around which symmetrical correlation peaks are expected to appear. Typical F−F distances are ∼2.8 Å for F_B−F_B, F_B−F_D, and F_D−F_D, and ∼3.2 Å for F_C−F_C, F_C−F_D, and F_D−F_D. All F−F distances involving F_A are greater than 4.7 Å, as is the F_B−F_C distance. (b) An expansion of the clinohumite structure showing the through-space proximity between two F_B species, and the substitution of one hydroxyl group (indicated with *) by fluorine to produce an F_B−F_D proximity. Fluorine, oxygen, magnesium, and hydrogen/deuterium are shown in pink, red, green, and black, respectively.

transferred between distinct fluorine species, were performed. Figure 4a shows a ^{19}F DQ MAS spectrum of $F_{0.5}(OD)_{0.5}$-clinohumite, recorded with ν_R = 30 kHz, using BABA recoupling. This experiment correlates homonuclear dipolar-coupled spin pairs and thus identifies fluoride ions that are in close spatial proximity. The use of only one cycle of recoupling limits the correlations observed in the spectrum to those between spins that share a relatively large dipolar coupling. The observation of correlation peaks (and therefore of magnetization transfer between fluoride ions) confirms that the spectral resonances result from species that coexist in the same disordered phase. Furthermore, the cross-peaks present support the spectral assignment resulting from the DFT calculations. An autocorrelation peak corresponding to a F_B−F_B proximity, observed at δ_{DQ} = −338.6 ppm, is expected from an arrangement such as that shown in Figure 4b, where two F_B sites are separated by a distance of ∼2.7 Å (determined from an computationally optimized structure containing this arrangement). Substitution of a further hydroxyl group by fluorine in this arrangement would lead to a F_B−F_D proximity, as shown in Figure 4 b, and a corresponding correlation is observed in the spectrum at δ_{DQ} = −347.0 ppm. Weaker correlations are also seen between F_C−F_C, F_C−F_D, and F_D−F_D. The low relative intensities of these correlations is partly attributable to the lower populations of these sites as observed in the ^{19}F MAS NMR spectrum in Figure 2. No correlations are observed between the ^{19}F resonances with

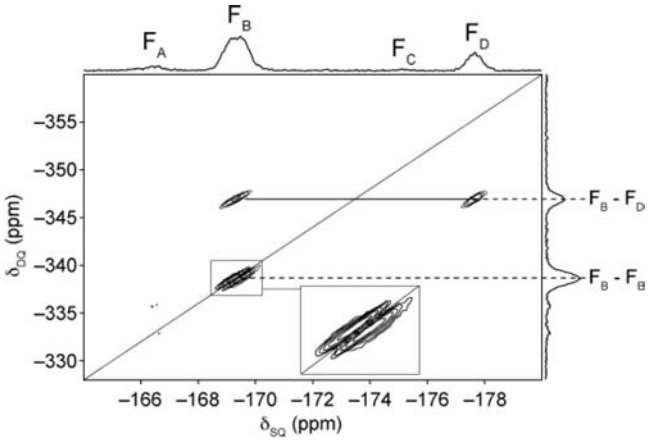

Figure 5. ^{19}F through-bond DQ MAS NMR spectrum, and corresponding projections, of $F_{0.5}(OD)_{0.5}$-clinohumite, recorded using a refocused-INADEQUATE pulse sequence, with $\nu_R = 30$ kHz. The diagonal line shows the axis $\delta_{DQ} = 2\delta_{SQ}$, around which symmetrical correlation peaks are expected to appear. The inset shows an expanded view of the F_B-F_B correlation peak.

$\delta = -169.3$ and -175.1 ppm, confirming these as F_B and F_C species (as these two local environments cannot exist in close proximity, as shown in Figure 3b). It is also noteworthy that no significant correlations are observed involving F_A; this is consistent with this site being surrounded by hydroxyl groups and therefore having no fluorine nearest neighbors.

Figure 5 shows a ^{19}F DQ MAS spectrum of $F_{0.5}(OD)_{0.5}$-clinohumite, recorded with $\nu_R = 30$ kHz, using a refocused-INADEQUATE pulse sequence, where magnetization is expected to be transferred through the scalar coupling. Intense F_B-F_B and F_B-F_D correlation peaks are also observed in this spectrum, although correlations involving F_C and F_D are of very low intensity (below the contour level shown). This may result either from differences in the optimum DQ excitation τ interval required (as the scalar coupling varies) or perhaps, more likely, to increased T_2 relaxation as a result of the fluorine-rich local environment which results in larger dipolar couplings. Although autocorrelation peaks (i.e., those between crystallographically identical species) lying along the $\delta_{DQ} = 2\delta_{SQ}$ diagonal are not normally expected to appear in spectra where magnetization transfer takes place via the scalar coupling, close inspection of the F_B-F_B autocorrelation peak at $\delta_{DQ} = -338.6$ ppm reveals that it has a doublet-like structure with a splitting of 0.3 ppm in the F_2 dimension. Given the disordered nature of the material, this can be attributed to differences in the long-range environment of the F_B species within a pair, resulting in nonidentical isotropic chemical shifts. This is consistent with the calculated isotropic chemical shifts for $2 \times 1 \times 1$ and $3 \times 1 \times 1$ supercells, which show differences of up to 0.2 ppm between adjacent F_B sites in an F_B-F_B pair. The doublet-like splitting of the F_B-F_B autocorrelation peak is also observed in the ^{19}F dipolar DQ MAS NMR spectrum in Figure 4a; however, it is less obvious owing to an overlapping correlation peak on the $\delta_{DQ} = 2\delta_{SQ}$ diagonal which corresponds to proximate F_B sites that do have precisely the same isotropic chemical shift.

The refocused-INADEQUATE experiment has been used extensively to probe through-bond connectivities in a wide range of materials, including, for example, $^{13}C-^{13}C$ connectivities in organic materials, $^{31}P-O-^{31}P$ connectivities in phosphate glasses and $^{29}Si-O-^{29}Si$ connectivities in framework materials and silicates.[28−31] A key assumption in the use of this experiment is that the effect of the homonuclear dipolar coupling is removed by MAS, such that any DQ coherence created results only from nuclei connected by a scalar coupling. This approach is rarely used, therefore, for the study of high-γ nuclei with high natural abundance, such as ^{1}H or ^{19}F, where spectra are often dominated by strong dipolar couplings, resulting in some doubt as to the origin of the correlation peaks observed. It is expected, however, that dipolar couplings will be efficiently removed at sufficiently rapid sample rotation rates. For $F_{0.5}(OD)_{0.5}$-clinohumite, very similar resolution is obtained in the ^{19}F MAS NMR spectrum for MAS rates of 30 and 60 kHz, suggesting that there is little significant contribution from dipolar couplings in either case. Furthermore, a ^{19}F DQ refocused-INADEQUATE spectrum recorded with $\nu_R = 60$ kHz also exhibits similar correlation peaks to those in Figure 5, confirming that these result from scalar, rather than dipolar, couplings. For further details of these experiments, see Supporting Information. It has been shown, however, that refocused-INADEQUATE spectra of solids may contain anomalous or unexpected correlation peaks between pairs of nuclei with a spatial (rather than through-bond) proximity, owing to a $n = 0$ rotational resonance condition.[20] Such correlations may be observed for dipolar-coupled spins that have similar isotropic chemical shifts but have CSA tensors with different magnitudes or orientations, provided that the MAS rate is comparable to or smaller than the CSA. The intensity of these anomalous peaks decreases with faster MAS rates, thus enabling them to be distinguished from those correlations resulting purely from scalar couplings.[20] However, Table 1 shows that the (average) calculated CSA values for the four ^{19}F species in $F_{0.5}(OD)_{0.5}$-clinohumite are between 5 and 9 ppm, corresponding to between 3 and 6 kHz at 14.1 T, much smaller than the MAS rates employed experimentally. (Note it is not possible to obtain experimental CSA values owing to the strong dipolar couplings present when the MAS rate is low). Furthermore, no significant differences are observed in the relative intensities of the correlation peaks in the refocused-INADEQUATE spectrum with $\nu_R = 60$ kHz (see Supporting Information), again suggesting that they result from scalar, rather than dipolar couplings.

Although the correlation peaks in Figure 5 result from scalar couplings between ^{19}F species, direct experimental measurement of such couplings in solids is often difficult, as they are rarely resolved in MAS spectra owing to the broader experimental line widths. However, it is often possible to measure scalar couplings in solids using a *J*-resolved experiment,[21] where a simple spin echo is utilized to refocus evolution due to all linear terms in the NMR Hamiltonian (i.e., those that resemble resonance offsets such as magnetic field inhomogeneity or disorder). In this way, it is possible to obtain refocused line widths that may be sufficiently narrow as to allow the observation of splittings due to the smaller scalar couplings. This approach has been used for the study of $^{31}P-^{31}P$ *J* couplings in organometallic compounds,[32,13] $C-^{13}C$ couplings in organic materials,[33] and more recently for the study of $^{29}Si-O-^{29}Si$ *J* couplings in crystalline and glassy silicates.[31] Figure 6 shows

(28) (a) Lesage, A.; Bardet, M.; Emsley, L. *J. Am. Chem. Soc.* **1999**, *121*, 10987. (b) Holland, G. P.; Jenkins, J. E.; Creager, M. S.; Lewis, R. V.; Yarger, J. L. *Chem. Commun.* **2008**, 5568. (c) Harris, R. K.; Joyce, S. A.; Pickard, C. J.; Cadars, S.; Emsley, L. *Phys. Chem. Chem. Phys.* **2006**, *8*, 137.
(29) O'Dell, L. A.; Guerry, P.; Wong, A.; Abou Neel, E. A.; Pham, T. N.; Knowles, J. C.; Brown, S. P.; Smith, M. E. *Chem. Phys. Lett.* **2008**, *455*, 158.
(30) Cadars, S.; Brouwer, D. H.; Chmelka, B. F. *Phys. Chem. Chem. Phys.* **2009**, *11*, 1825.
(31) Florian, P.; Fayon, F.; Massiot, D. *J. Phys. Chem. C.* **2009**, *113*, 2562.

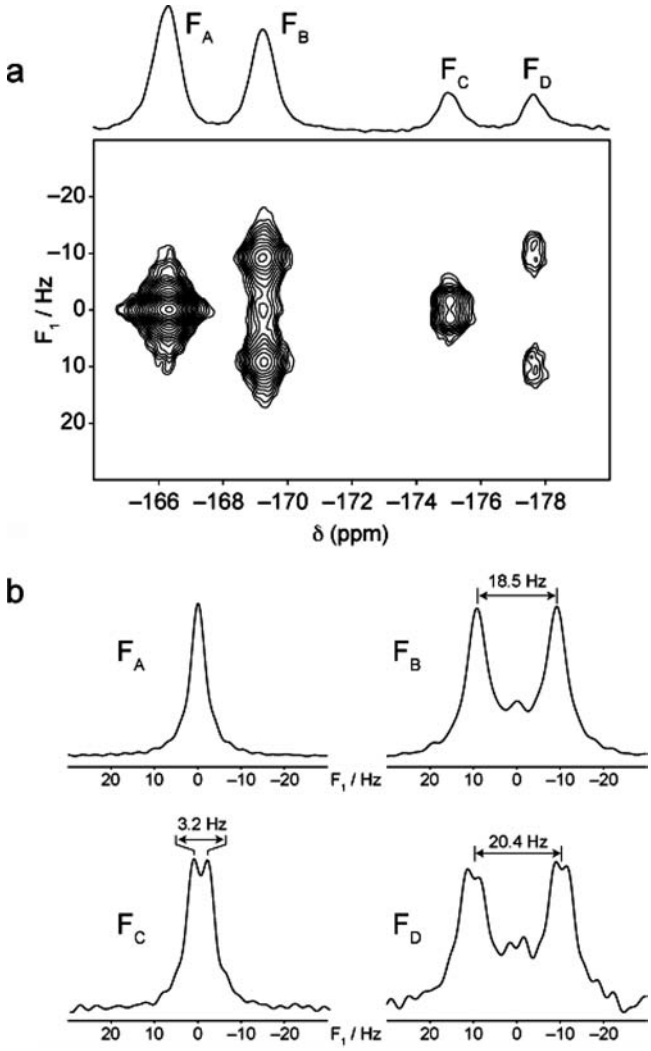

Figure 6. (a) ^{19}F *J*-resolved spectrum, and F_2 projection, of $F_{0.5}(OD)_{0.5}$-clinohumite, recorded with $\nu_R = 60$ kHz. (b) Projections taken parallel to F_1, across each of the four fluorine resonances.

a ^{19}F *J*-resolved spectrum of $F_{0.5}(OD)_{0.5}$-clinohumite, recorded with $\nu_R = 60$ kHz, and corresponding projections parallel to F_1, for each fluorine species. As shown in Figure 6b, a splitting of ∼18.5 Hz is observed for F_B, with a much smaller splitting (of ∼3.2 Hz) present for F_C. F_D exhibits a slightly larger splitting of ∼20.4 Hz, with evidence of a more complex multiplet structure, perhaps associated with the two *J* couplings expected for this site. Notably, no splitting or broadening is observed for F_A, which has no fluorine nearest neighbors. Despite the use of rapid MAS, it is possible that residual dipolar couplings may still contribute to the spectrum if the spinning angle is not accurately adjusted.[34] Owing to the magnitude of the homonuclear dipolar coupling, even a small deviation of the spinning angle away from 54.736° could introduce a residual coupling

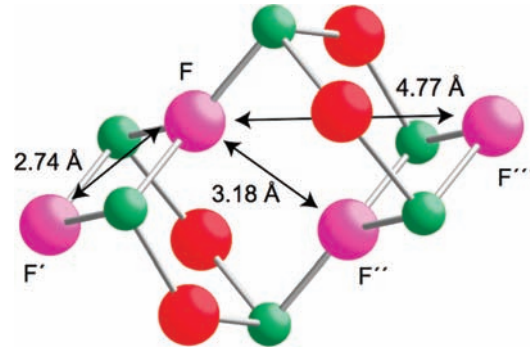

Figure 7. An expanded view of the structure of fully fluorinated clinohumite, showing distances between adjacent fluorine sites. Fluorine, oxygen, and magnesium are shown in pink, red, and green, respectively.

of sufficient magnitude to affect the splittings observed in a *J*-resolved experiment. Cross-sections extracted from *J*-resolved spectra of $F_{0.5}(OD)_{0.5}$-clinohumite for F_B as the spinning angle is varied over the range 54.736° ± 0.04° reveal that the observed splitting indeed changes, confirming the reintroduction of a small residual dipolar interaction. When the spinning angle is accurately adjusted, however (as measured by the line width of the OD resonance in the ^{2}H MAS NMR spectrum of malonic acid), a splitting is still observed (∼18.2 Hz), which results entirely from the scalar coupling. See Supporting Information for more details.

The observation of scalar couplings between two species usually indicates a significant through-bond interaction between them, mediated by the covalent bonding electrons. The expanded view of the structure of a (geometry optimized) fully fluorinated clinohumite, shown in Figure 7, indicates there are two possible through-bond pathways between adjacent F species, via a notional two-bond F−Mg−F′ interaction or a notional four-bond F−Mg−O−Mg−F′ interaction. This agrees reasonably well with the experimental observation of two couplings of different magnitude (average splittings in Figure 6b of ∼18.5 and ∼3.2 Hz, respectively). The local fluorine environments shown in Figure 3b demonstrate that the larger (two-bond) interaction is expected to be present for F_B, while F_C would exhibit only the smaller (four-bond) coupling. In contrast, both interactions should affect F_D, while F_A has no fluorine neighbors at all. However, the F−Mg interaction in this structure is expected to be mostly ionic in character, with a large electronegativity difference (3.98 for F and 1.31 for Mg) between the two. Indeed, DFT calculations performed on the model structures considered in this work give F−Mg bond overlap populations of between 0.17 and 0.19, which are similar to values calculated for NaCl and NaF,[35] suggesting a similar degree of ionicity. At first sight, therefore, it is perhaps surprising that scalar couplings are observed at all. In this context, it is significant that a number of solution-state NMR studies have reported the existence of so-called "through-space" J_{FF} couplings, where the indirect nuclear spin−spin coupling interaction is observed between sites that are in close spatial proximity but are not bonded through formal chemical bonds.[36,37] The mechanism of this interaction is thought to be via direct overlap of orbitals occupied by fluorine lone pairs. This is distinguished from the direct dipolar

(32) (a) Wu, G.; Wasylishen, R. E. *Organometallics* **1992**, *11*, 3242. (b) Eichele, K.; Wu, G.; Wasylishen, R. E. *J. Magn. Reson.* **1993**, *101*, 157. (c) Wu, G.; Wasylishen, R. E. *J. Chem. Phys.* **1993**, *98*, 6138. (d) Wu, G.; Wasylishen, R. E. *Inorg. Chem.* **1996**, *35*, 3113.
(33) (a) Cadars, S.; Lesage, A.; Trierweiler, M.; Heux, L.; Emsley, L. *Phys. Chem. Chem. Phys.* **2007**, *9*, 92. (b) Brown, S. P.; Emsley, L. *J. Magn. Reson.* **2004**, *171*, 43. (c) Cadars, S.; Lesage, A.; Hedin, N.; Chmelka, B.; Emsley, L. *J. Chem. Phys. B.* **2006**, *110*, 16982.
(34) Pileio, G.; Guo, Y.; Pham, T. N.; Griffin, J. M.; Levitt, M. H.; Brown, S. P. *J. Am. Chem. Soc.* **2007**, *129*, 10972.
(35) Segall, M. D.; Shah, R.; Pickard, C. J.; Payne, M. C. *Phys. Rev. B* **1996**, *54*, 16317.
(36) Wasylishen, R. E. In *Encylopedia of Nuclear Magnetic Resonance*; Grant, D. M.; Harris, R. K., Eds.; Wiley: Chichester, 1996.
(37) Bryce, D. L.; Wasylishen, R. E. *J. Mol. Struct.* **2002**, *602*, 463.

Table 2. Calculated Isotropic, J_{iso}, Its Division into the Four Contributions (Fermi contact, FC, Spin-Dipolar, SD, Paramagnetic Spin-Orbital, PSO, and Diamagnetic Spin-Orbital, DSO) Together with the Anisotropic Term, ΔJ, for the $^{19}F-^{19}F$ J Coupling in the Geometry-Optimized Structure of a $3 \times 1 \times 1$ Supercell of Fully Fluorinated Clinohumite ($4Mg_2SiO_4 \cdot MgF_2$), Shown in Figure 7

	contribution to J_{iso}/Hz					
	FC	SD	PSO	DSO	J_{iso}/Hz	ΔJ/Hz
J(F−F′)	16.05	3.89	−33.68	2.50	−11.23	224.15
J(F−F″)	1.30	1.22	−8.56	2.48	−3.56	41.38

coupling interaction which, although a through-space interaction, does not involve intervening electrons. From Figure 7, it is apparent that adjacent fluorines are separated by approximately 2.7 and 3.2 Å, distances that are only slightly greater than the sum of the ionic radii (1.33 Å) of the two fluoride anions. It may be postulated that such "through-space" interactions may provide an additional (or even alternative) mechanism for the observation of scalar couplings in humites.

Evidence for "through-space" J_{FF} couplings comes from a large number of studies. For example, unusually large $^{19}F-^{19}F$ J couplings have been seen in difluoronaphthalene and difluorophenanthrene derivatives, where two fluorines that are separated by several bonds are forced into close proximity by the molecular geometry.[38] In a study of a dihydrofolate reductase−NADPH−MTX complex, a 17.2 Hz J coupling was seen between two fluorines, which are separated by 398 bonds but are held in close proximity due to the folding of the protein.[39] A significant "through-space" component for this interaction has been more recently identified in a DFT study of the same system.[40] Furthermore, an ab initio investigation of $^{19}F-^{19}F$ scalar couplings in model systems comprising hydrogen fluoride and fluoromethane showed that significant couplings are expected when nuclei are separated by the sum of their van der Waals radii.[37] The magnitude of the coupling interaction is strongly dependent on the geometrical arrangement and the overlap integrals of the fluorine orbitals. The experimental observation of two different couplings for $F_{0.5}(OD)_{0.5}$-clinohumite, therefore, could reflect the two different distances between fluorine species (i.e., ∼2.7 Å for F/F′ and 3.2 Å for F/F″) and two differing through-space contributions.

In order to gain further insight into the origin of the J couplings observed in this work, DFT calculations were performed for a $3 \times 1 \times 1$ supercell of fully fluorinated clinohumite. The isotropic contribution to the J couplings can be considered as arising from four distinct contributions: the Fermi contact (FC) and spin-dipolar (SD) contributions are due to the polarization of the electron spin, and the two spin−orbital contributions, diamagnetic (DSO) and paramagnetic (PSO), are due to induced orbital currents. Table 2 gives the calculated contributions of these components to the isotropic J coupling (J_{iso}) for J(F−F′) and J(F−F″). The J(F−F′) coupling has large spin and orbital contributions, which are of opposite sign and partially cancel, giving an isotropic J coupling of −11.23 Hz. However, the anisotropic J coupling, ΔJ, for this interaction (also shown in Table 2) is much larger, indicating that the principal components of the tensor must also be large and be of opposite sign (see Table S4 in Supporting Information). The J(F−F′) coupling is much smaller ($J_{iso} = -3.56$ Hz), although ΔJ is again an order of magnitude larger. The prediction of these couplings presents strict demands on the fidelity of the calculations, first because the total J arises from essentially the sum of two contributions which partially cancel and, second, because the corresponding reduced coupling constant, K, is rather small. In a quantum mechanical calculation, K is the quantity which is directly computed; the large J(F−F) coupling is in part due to the large gyromagnetic ratio for ^{19}F (note that $J_{AB} = (\hbar\gamma_A\gamma_B/2\pi)\,K$, where γ_A and γ_B are the gyromagnetic ratios of nuclei A and B, respectively). The prediction of two significant J couplings of differing magnitude is in good agreement with the experimental observations. Perfect agreement would not be expected however, as, in contrast to the ordered fully fluorinated structure which was used in the calculation, the disorder in the real structure will lead to a distribution of environments and a distribution of J couplings, as observed experimentally in the J-resolved spectrum in Figure 6. It can be seen from Table 2 that although the magnitudes and signs of the Ramsey contributions to J are comparable to quantum chemical studies of "through-space" J(F−F) couplings in organic compounds,[39] we find that the PSO contribution is larger than the FC which results in a negative total J (note that the experiments provide only the magnitude of J). However, Figure 7 shows that in addition to the F−F‴ interaction, there is a similar "four-bond" pathway between F and F″. Although connected through a similar number of "bonds", these two F species are spatially much more distant (∼4.8 Å), considerably diminishing the likelihood of any "through-space" interaction. It is significant, therefore, that the calculated coupling between this pair of fluorines is very close to zero ($J_{iso} = -0.4$ Hz and $\Delta J = -0.2$ Hz), suggesting that there is a through-space contribution to the J(F−F′) and J(F−F″) couplings.

The ^{19}F NMR spectra of $F_{0.5}(OD)_{0.5}$-clinohumite appear to show that, although fluorine substitution results for the most part in the formation of OD···F^- hydrogen-bonded pairs, there is long-range disorder in the structure, and a small proportion of fluorines are not involved in hydrogen bonds at all. However, the material considered here has been produced synthetically, while many of the previous diffraction studies have been carried out on natural clinohumite ($4Mg_2SiO_4 \cdot Mg(F,OH)_2$), with varying levels of fluorine substitution. It is not clear whether the disorder observed in our synthetic sample would necessarily be present in natural samples that have been formed over much longer time periods under very different conditions. The study of natural minerals by NMR is often hampered, or indeed prohibited, by the presence of iron in the structure which gives rise to a significant paramagnetic broadening of the spectral resonances. However, at some geographical locations natural clinohumite exists with a very low iron content, offering the possibility of NMR investigation. A natural gem-quality crystal, with chemical composition $Mg_{8.85}Fe_{0.01}Ti_{0.2}(Si_{3.94}O_{16})O_{0.4}F_{0.97}(OH)_{0.63}$, from Pamir, Tajikistan, was purchased commercially in order to investigate the number and type of F environments present. This material has a similar but slightly higher level of fluorine substitution to our synthetic clinohumite but is also substituted by titanium. Substitution of Mg^{2+} by Ti^{4+} (and the concomitant removal of two H^+) results in the presence of a single H site in Ti-substituted clinohumite and the avoidance of potentially destabilizing H···H interactions.[41] Figure 8a shows a ^{19}F MAS NMR spectrum of natural clinohumite, recorded with $\nu_R = 60$ kHz. Although the observed line widths

(38) Mallory, F. B.; et al. *J. Am. Chem. Soc.* **2000**, *122*, 4108.
(39) Kimber, B. J.; Feeney, J.; Roberts, G. C. K.; Birdsall, B.; Griffiths, D. V.; Burgen, A. S. V.; Sykes, B. D. *Nature* **1978**, *271*, 184–185.
(40) Arnold, W. D.; Mao, Junhong, M.; Sun, H.; Oldfield, E. *J. Am. Chem. Soc.* **2000**, *122*, 12164.
(41) Berry, A. J.; James, M. *Mineral. Mag.* **2000**, *66*, 441.

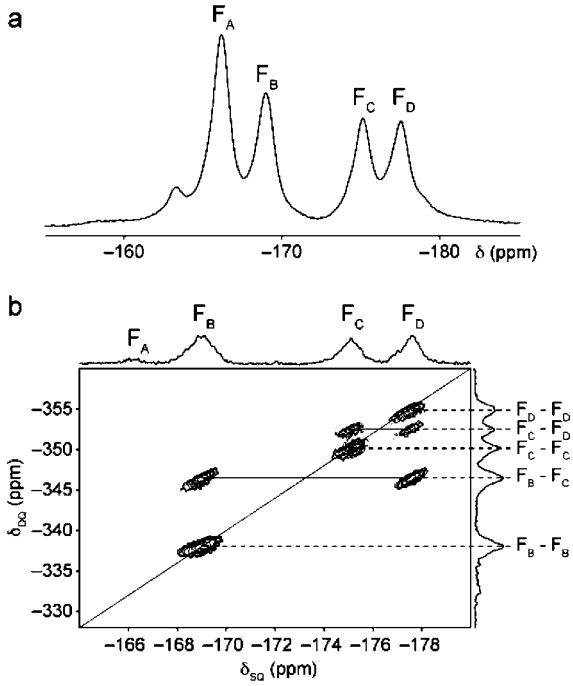

Figure 8. (a) ^{19}F MAS NMR spectrum of a natural clinohumite sample with composition $Mg_{8.85}Fe_{0.01}Ti_{0.2}(Si_{3.94}O_{16})O_{0.4}F_{0.97}(OH)_{0.63}$, recorded with $\nu_R = 30$ kHz. (b) Rotor-synchronized ^{19}F through-space DQ MAS NMR spectrum of natural clinohumite, and corresponding projections, recorded using one cycle of BABA recoupling, with $\nu_R = 30$ kHz. The diagonal line shows the axis $\delta_{DQ} = 2\delta_{SQ}$, around which symmetrical correlation peaks are expected to appear.

are broader, presumably owing to the small amounts of iron present in the sample, four major ^{19}F resonances are observed at the same chemical shifts as those found in synthetic $F_{0.5}(OD)_{0.5}$-clinohumite, confirming the presence of significant disorder in the material. A fifth weak resonance at −163.3 ppm is probably due to F species which are also close to the Ti present in the crystal structure. As observed previously, the resonances corresponding to F_A and F_B are the most intense, although the relative intensities of F_C and F_D are higher than in the synthetic sample, indicating larger fluorine-rich regions. This is perhaps to be expected, as regions where Ti substitution is higher will presumably have lower fluorine content, leaving the remainder of the material more fluorine rich. The ^{19}F (dipolar) DQ MAS NMR spectrum, shown in Figure 8b, is very similar to that observed for synthetic $F_{0.5}(OD)_{0.5}$-clinohumite in Figure 4a, with significantly more intense F_C-F_C, F_C-F_D, and F_D-F_D correlation peaks. A ^{19}F *J*-resolved spectrum of natural clinohumite is shown in Figure 9. Although the projections for each fluorine site are significantly broader (attributed to increased T_2 relaxation due to the small amount of iron present), the spectrum is similar to that of synthetic $F_{0.5}(OD)_{0.5}$-clinohumite in Figure 6. Splittings are evident for F_B and F_D, of ∼14 Hz, although it is not possible to determine whether there is a smaller splitting for F_C due to the larger line widths. In general, ^{19}F NMR spectra show a similar range of F environments for both natural and synthetic clinohumite, suggesting that sample preparation is not a contributing factor to the structure and order observed.

Conclusions

We have demonstrated the use of high-resolution ^{19}F MAS NMR spectroscopy to study disorder and bonding in clinohumite, a mineral of considerable interest as a model for the incorporation of water within the Earth's mantle. We have

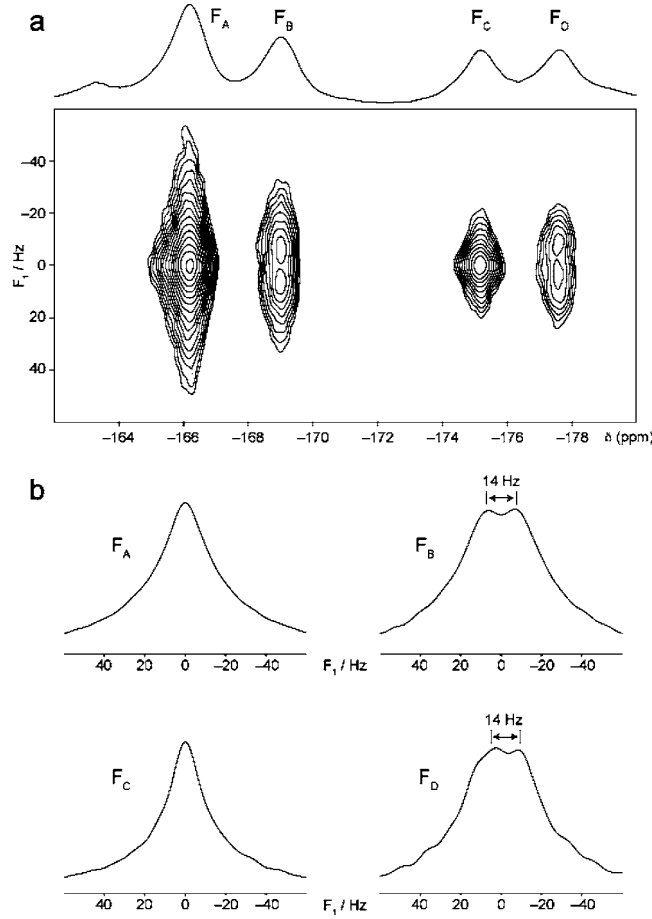

Figure 9. (a) ^{19}F *J*-resolved spectrum, and F_2 projection, of $F_{0.5}(OD)_{0.5}$-clinohumite, recorded with $\nu_R = 60$ kHz. (b) Projections taken parallel to F_1, across each of the four fluorine resonances.

shown that there is extensive structural disorder, with four distinct fluorine environments observed in the ^{19}F MAS NMR spectrum. This disorder is observed for both natural clinohumite and for a synthetic fluorine-substituted deuterated clinohumite. Using first-principles DFT calculations we have been able to identify the local environment of each fluorine species, as the observed chemical shift appears to be dominated by the nature of the species (i.e., F^- or OD^-) on the two nearest anion sites. However, our results also show that in order to accurately predict ^{19}F chemical shifts, a scaling factor (of 0.68) must be applied to the calculated isotropic shieldings. This was determined by consideration of the ^{19}F chemical shifts for 20 simple fluorine-containing solids. The assignment and interpretation of the ^{19}F MAS NMR spectrum is supported by two-dimensional ^{19}F DQ MAS NMR experiments that correlate fluorine resonances based on either through-space or through-bond connectivity. The observation of ^{19}F−^{19}F *J* coupling-mediated correlations is perhaps surprising, as the fluorines in the structure are connected by F−Mg−F or F−Mg−O−Mg−F linkages, and the Mg−F interaction is expected to be primarily ionic in character. However, significant scalar couplings are also calculated using DFT and are in good agreement with the splittings observed in experimental *J*-resolved spectra. While it is difficult to unambiguously identify the mechanism mediating the coupling, the observation of significant couplings only between F which are close in space and not those which have similar "through-bond" connectivity but are spatially remote suggests that there is a "through-space" contribution to the interactions observed. This

finding has important implications for the interpretation of NMR experiments where magnetization is assumed to be transferred by interactions thought to exist only between species with a formal covalent (or hydrogen) bond, raising the question of how the nature of bonding in the solid state should be described.

Acknowledgment. We are grateful to EPSRC for support (Grant No. EP/E041825) and to the research councils for an RCUK Academic Fellowship to SEA. This research has also made use of the resources provided by the EaStCHEM Research Computing Facility (http://www.eastchem.ac.uk/rcf); this facility is partially supported by the eDIKT initiative. J.R.Y. thanks the Royal Society for funding, and the Oxford Supercomputer Centre for computing facilities. Antony Burnham and John Spratt are thanked for the electron microprobe analyses.

Supporting Information Available: Additional experimental solid-state NMR details, further information on ^{19}F DFT calculations, and fast spinning ^{19}F MAS NMR spectra. This material is available free of charge via the Internet at http://pubs.acs.org.

JA105347Q